Hemodynamics in Multiple Intracranial Aneurysms: The Role of Shear Related to Rupture

P. Berg, G. Janiga, O. Beuing, M. Neugebauer, and D. Thévenin

***Abstract*—Wall shear stress is the most prominent hemodynamic parameter associated with intracranial aneurysm rupture. Since low as well as high shear theories still coexist, the aim of this study was to investigate several shear related variables on datasets with multiple intracranial aneurysms.**

Therefore, two patient-specific anterior circulations of the human cerebral vascular system were reconstructed, containing two and three intracranial aneurysms, respectively. The hemodynamic simulations are based on flow rates measured by means of 7-Tesla PC-MRI. Since a rupture occurred in both cases and the affected aneurysms could be identified, the evaluation of time-averaged wall shear stresses, their gradients as well as the oscillatory shear indices mainly focuses on a comparison between ruptured and unruptured aneurysms.

Areas of low and elevated shear were found in all cases and no correlation with rupture was identified. However, the ruptured aneurysms feature significantly higher directional changes of the shear vector associated to a stronger flow oscillation. This observation suggests that a combination of low average shear stresses wit increased oscillations is present in ruptured aneurysms. In that case, wall shear stress cannot be used exclusively in order to predict the rupture probability and the oscillatory shear index should be taken into account, probably as one of several additional indicators.

***Index Terms*—CFD, hemodynamics, intracranial aneurysms, wall shear stress.**

I. Introduction

Intracranial aneurysms are vascular dilatations typically located in the Circle of Willis (CoW), which supplies blood to the brain and ensures an unhindered blood flow into all areas. They occur in approximately 1-7% of the western population [1]-[3]. Their incidence is difficult to estimate because various aneurysms remain undetected until first neurological symptoms set in. Rates of rupture are reported to be in a range between 8 – 10 cases per 100,000 persons per year [4]-[6] depending on age, gender, origin and genetic conditions. Although these rates are relatively low the outcome can be lethal (45-75% [7]) or connected to high morbidity in case of missing medical care. Multiple cerebral aneurysms develop in 15% to 33% of affected persons, increasing the probability of a potential rupture [8]-[12]. In patients presenting with subarachnoid hemorrhage multiple aneurysms are even diagnosed in up to 45% of all cases [13]-[15].

Cases with more than one aneurysm might be associated with a higher chance of detecting reasons for the rupture of cerebral dilatations. Within the last decades, several groups have been using computational methods in order to extract parameters explaining aneurysmal formation or predicting rupture probabilities [16]-[18]. However, those investigations mainly focus on single aneurysm models using various assumptions and leading to controversial discussions [19]. Typically, just the pathological area in combination with short distal and proximal branches is considered, which results in shorter simulation times but also in a stronger influence of the applied boundary conditions. In contrast, Alastruey *et al.* [20] modeled the CoW by simulating different scenarios of vessel occlusion. But due to a 1-D approach no hemodynamic flow patterns can be extracted to indicate the ignition of vascular malformations.

Since Castro et al. [21] observed a significant impact of the parent artery segmentation on intra-aneurysmal hemodynamics it is important to include as much geometric information as possible. Additionally, synthetic boundary conditions may lead to unrealistic blood flow predictions [22].

Therefore, Zuleger *et al.* [23] measured time-dependent velocity fields by means of 4D phase-contrast magnetic resonance angiography (PC-MRA) in order to carry out blood flow simulation in a whole model of a healthy CoW. Regions of typical aneurysm locations were examined in more detail to identify flow parameters that might be in correlation with a possible formation. High average wall shear stress gradients were detected in common aneurysm areas but no diseased case was considered as comparison.

Within the present study two patient-specific data sets are investigated containing two and three intracranial aneurysms, respectively. The complete affected anterior circulation was reconstructed in both cases, providing a wider computational domain. In order to achieve realistic inflow conditions 7-Tesla PC-MRI measurements were carried out and applied to the internal carotid arteries.

The purpose of this study is to contribute to the understanding of the hemodynamics in the diseased human CoW under realistic conditions. In addition, parameters that are associated with aneurysmal initiation, growth and rupture are analyzed as well as evaluated. The focus lies especially on the influence of shear on the endothelial layer whereby its

Manuscript received November 10, 2012; revised February 24, 2013. This work was supported in part by the International Max Planck Research School for Analysis, Design and Optimization in Chemical and Biomedical Process Engineering Magdeburg.

P. Berg, G. Janiga, and D. Thévenin are with the Department of Fluid Dynamics and Technical Flows, University of Magdeburg, Germany (e-mail: Philipp.Berg@ovgu.de).

O. Beuing is with the Department of Neuroradiology, University Hospital of Magdeburg, Germany (e-mail: Oliver.Beuing@med.ovgu.de).

M. Neugebauer is with the Department of Simulation and Graphics, University of Magdeburg, Germany (e-mail: mathias@isg.cs.uni-magdeburg.de).

role related to a rupture probability will be discussed in detail. In consequence, a better understanding of the biomechanical processes would support every attending practitioner.

II. Methods and Materials

A. Vascular Models

In order to carry out the desired blood flow simulations it was necessary to generate suitable geometry models. Therefore, clinical image data were acquired by means of 3D rotational angiography providing the basis to obtain three-dimensional data of cerebral arteries. The segmentation of the aneurysm geometry was performed using a threshold followed by a connected component analysis. A Marching Cubes algorithm finally reconstructed the segmented mask data. A preprocessing on the resulting mesh allows for an artifact reduction with sub-voxel precision. This includes artifacts like vessel-blending, surface noise or narrow vessel segments [24]. They are caused by the partial-volume effect, unfavorable contrast agent distribution or physical effects during the CT-scan process. To achieve a high surface quality the segmentation results were transformed into discrete meshes and smoothed afterwards [25].

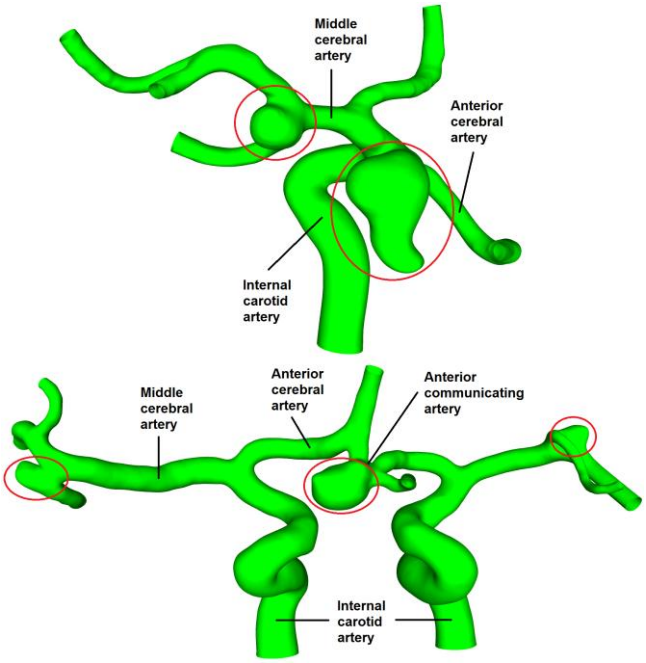

Fig. 1. Patient-specific smoothed surfaces of the vascular models: case a with a MCA and an ICA aneurysm (top), case b with two MCA and an AcomA aneurysm (bottom).

The resulting surface meshes represent the anterior circulations of the CoW. Fig. 1 presents the shapes of the investigated geometries from an anterior view. The inflow regions are positioned at the bottom and described by the internal carotid arteries (ICA). All investigated intracranial aneurysms are highlighted whereby case A contains one aneurysm at the ICA bifurcation and a second at the middle cerebral artery (MCA). Mean diameters are 6.5 mm and 3.9 mm, respectively. In case B two MCA aneurysms (2.8 mm, 2.6 mm) and one at the anterior communicating artery (AcomA - 5.3 mm) were diagnosed.

Before the final hemodynamic simulations were performed, the computational domain was discretized. This resulted in four unstructured volume meshes per case consisting of tetrahedral cells. The commercial software ANSYS ICEM-CFD® 14.0 (Ansys Inc., Canonsburg, PA, USA) was used for the spatial discretization. A Delaunay method created the tetrahedral elements with a maximum size ranging from 0.24 to 0.05 mm. In areas of strong changes in geometric direction, especially in regions of high curvature and close to the aneurysm sacs, local refinements of the meshes were carried out. Therefore, flow patterns are better resolved in these zones. Additionally, three boundary layers of prismatic elements were inserted to ensure a finer wall resolution and resolve the high velocity gradients close to the endothelial layer. Their initial height ranges from 32 to 13 µm and a growth ratio of 1.3 was defined. The number of elements varies between 450.000 and 10.1 million. To identify the influence of the mesh density several parameters were analyzed within a mesh independency study [26]. The resulting meshes, which were finally used, consist of 3.42 million elements in case A and 4.8 million in case B.

B. Hemodynamic Simulation

Based on the chosen meshes the unsteady hemodynamic simulation was carried out using the finite volume solver ANSYS Fluent® 14.0 (Ansys Inc., Canonsburg, PA, USA). Here, the integral formulations of the governing *Navier-Stokes* equations for continuity and momentum conservation are solved. Blood as a suspension of plasma and cellular components is treated as an isothermal, incompressible (ρ = 1055 kg/m^3) and Newtonian fluid with a constant dynamic viscosity $\eta = 4.265 \cdot 10^{-3}$ Pa·s [21]. Although the viscosity of blood can show a strong shear dependency, a comparison with the typically used *Carreau-Yasuda* model showed no significant difference in the velocity profiles for the present range of vessel diameters [27].

In contrast to analytically described inflow conditions (e.g., parabolic or *Womersley* profiles), which are generally based on numerous assumptions like flow in a cylindrical straight pipe, flow rates extracted from a 7-Tesla PC-MRI measurement of a healthy volunteer were implemented. This was carried out for the left as well as the right internal carotid artery and is presented for one cardiac cycle in Fig. 2. The time-dependent values were extracted from the raw image data using EnSight 9.2 (CEI Inc., Apex, NC, USA) and a post-processing tool developed by Stalder et al. [28]. The vessel walls are assumed to be rigid and no-slip boundary conditions are implemented. In contrast to significant vessel wall motions in the aortic arch, the radial dilatation of arteries in the CoW does not increase 5% of the diameter [29]. Additionally, aneurysm initiation is caused, inter alia, by elastin degradation in the media and adventitia vessel layer [30]. This leads to a decrease of flexibility and therefore, the assumption of non-flexible walls appears to be valid for this numerical investigation. For all outlets an outflow boundary condition is defined which weights the mass flow rates depending on each surface area. This method was chosen due to the lack of knowledge regarding the pressure variation in the different vessel branches.

In order to calculate the existing velocity fields within the domain, a pressure-implicit algorithm (PISO) was used for the unsteady simulations. Two steps of pressure correction were carried out within each loop. A constant time step size was chosen as 10^{-4} s according to the stability condition (Courant number < 1), which was estimated in advance. The gradients of the momentum equation are calculated using a least squares cell-based scheme. Laplacian as well as the convection terms are discretized by second order upwind schemes. Regarding the time discretization a second-order implicit scheme is applied.

Convergence was obtained when the scaled residuals of pressure and momentum decreased below a value of 10^{-5} within each time step. Due to the high number of elements the computational domain has been decomposed in advance in order to simulate in parallel. All simulations were carried out on 8 CPUs of the in-house cluster Kármán consisting of 544 computing cores (AMD Quad Core 2.1 GHz) and an InfiniBand network.

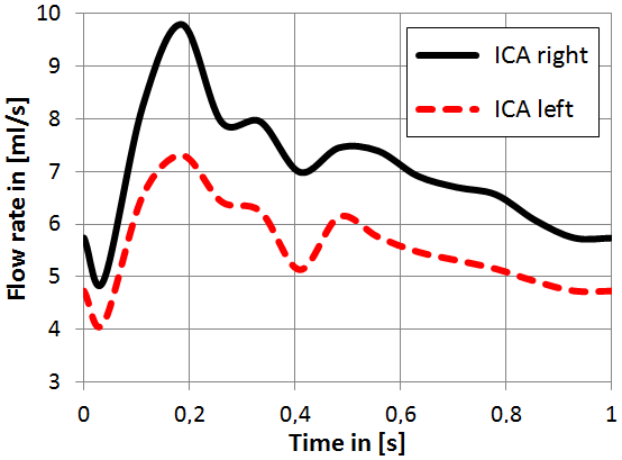

Fig. 2. Measured flow rates of one cardiac cycle (T=1 s) used as inflow boundary conditions for the numerical simulations: right (solid) and left (dashed) internal carotid artery. Peak systole appears at t = 0.186 s.

C. Analysis and Visualization

In the scope of this study most widely used indicators in hemodynamic post-processing like the maximum magnitude of the velocity vectors or highest wall shear stresses have been evaluated. In order to decrease numerical errors and achieve periodicity, only the third cardiac cycle is analyzed, discarding the first two cycles as initialization. A streamline-visualization at peak systole gives a first impression regarding the flow structure (see Fig. 3). To investigate unsteady effects appearing within one heartbeat, the parameters defined in Equations (1) to (3) are analyzed [31]. The time-averaged wall shear stresses (*AWSS*) as well as corresponding gradients (*AWSSG*) provide information regarding stressed regions on the arterial surface and may supply hints with respect to the rupture probability [23]. In addition, the oscillatory shear index (*OSI*) describes the directional change of the shear stresses for one cardiac cycle. The values of the resulting scalar field can range between 0 and 0.5 whereby higher values indicate increased fluctuation.

$$AWSS = \frac{1}{T} \cdot \int_0^T |\tau| \cdot dt \quad (1)$$

$$AWSSG = \frac{1}{T} \cdot \int_0^T \sqrt{|\nabla(\tau_x)|^2 + |\nabla(\tau_y)|^2 + |\nabla(\tau_z)|^2}\, dt \quad (2)$$

$$OSI = \frac{1}{2} \cdot \left(1 - \frac{\left| 1/T \cdot \int_0^T \tau \cdot dt \right|}{1/T \cdot \int_0^T |\tau| \cdot dt} \right) \quad (3)$$

III. Results

The obtained results for the five aneurysms are shown in Fig. 3. The two aneurysms of case A are presented in the first two columns, the three aneurysms of case B in the remaining three. The ICA aneurysm of the first case as well as the AcomA aneurysm of the second are characterized as ruptured and displayed in column 1 and 3, respectively. The visualization of the peak systolic streamlines demonstrates the formation of complex flow patterns within each aneurysm sack. In general, the development of at least one vortex can be detected due to the geometric conditions. This leads to a helical flow structure where the blood reenters into the parental artery through the ostium (surface area where the healthy vessel originally existed). This observation confirms the experience from several previous patient-specific vascular simulations whereby no difference between ruptured and unruptured cases can be recognized in the frame of this study.

However, considering the shear stresses, which are known to influence the endothelial cells of the inner vessel layer, significant differences are visible. With regard to the chosen legend scaling the ICA aneurysm of case A shows values which are generally lower than those of the surrounding arteries. In contrast to this situation, the unruptured aneurysm of the same case exhibits shear stresses which are equal or even higher than in healthy areas. The AcomA aneurysm of case B is a mixture of the first two showing the existence of decreased as well as increased shear areas. In the latter two cases low values are prominent in the dome region whereby the shear stress elevates with increasing proximity to the vessel. However, all five aneurysms have in common that the highest shear values occur distal and proximal of the dilatations. This is assumed to be caused by the interruption of the proper hemodynamic flow by the geometric remodeling. Due to the previously described findings, no clear correlation between the order of wall shear stress and the event of a rupture can be established. Therefore, neither the low nor the high shear theory can be supported or refuted with this analysis.

Concerning the wall shear stress gradients, it can be seen for all vessel dilatations that elevated values mainly occur close the aneurysmal neck regions. This can be indeed a dangerous area but the ruptures of both cases are rather observed at areas close to the dome.

Taking additionally into account the directional change of the wall shear stress for one cardiac cycle, several interesting observations can be drawn. For most parts of the healthy vascular system *OSI* does not exceed a value of 0.15. Elevated spots mainly occur on the aneurysmal sacks indicating that shear fluctuation is directly caused by the

diseased vessel regions. The ruptured aneurysm of each case possesses areas of high *OSI* whereas two unruptured MCA aneurysms show nearly no oscillation.

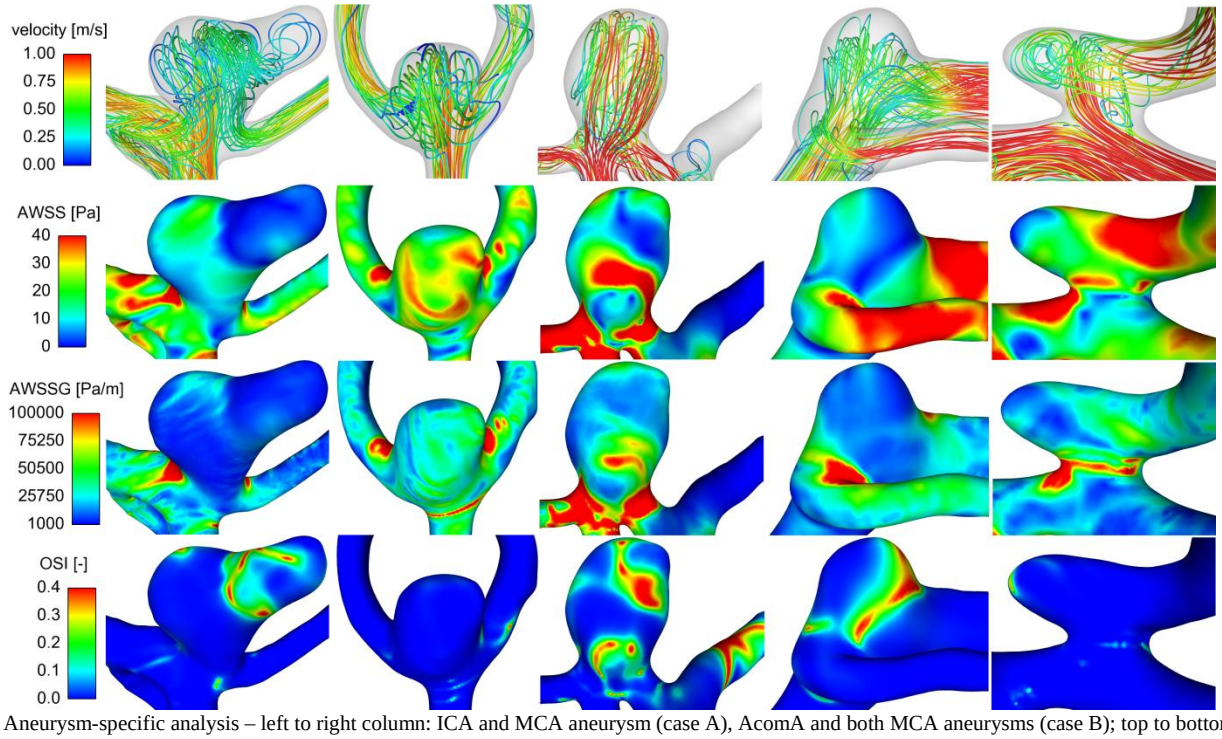

Fig. 3. Aneurysm-specific analysis – left to right column: ICA and MCA aneurysm (case A), AcomA and both MCA aneurysms (case B); top to bottom row: instantaneous streamline visualization at peak systole, temporal-averaged wall shear stresses (AWSS), temporal-averaged wall shear stress gradients (AWSSG), oscillatory shear index (OSI).

However, on one site of the third dilation, which did not rupture, increased *OSI* values appear as well. Therefore, a direct correlation between oscillating shear and the event of a rupture does not appear to hold in general.

IV. Discussion

The reported results reveal that due to remodeled cerebral vessel walls followed by the development of an aneurysmal dilatation disturbed flow features occur. Compared to a healthy vascular system such a flow behavior differs in a way that abnormal shear values may appear and influence the sensitive endothelial layer. Consequently, it can promote the degradation of affected wall areas. This process may hold until the media layer, responsible for the strength of the vessel, can no longer resist. In consequence, the weakened vessel rips letting the blood flow into the subarachnoid space.

Within this study it was neither possible to associate high shear stresses to the event of a rupture nor low values to the unruptured cases. The opposite does not hold either. This leads to the presumption that the hemodynamic parameter *AWSS* is not or at least not the only reason for a rupture. Hence, neither the low shear theory [18], nor those claiming high shear is responsible for rupture [5] can be confirmed.

Considering the directional changes of the shear vector for one cardiac cycle, one can see increased values of *OSI* in both ruptured aneurysms. However, the analysis also showed higher values of *OSI* on the side of one unruptured case. Again, no one-to-one correlation between *OSI* and rupture is possible in this study. Nevertheless, the latter aneurysm, classified as unruptured, may have been the next candidate for an imminent rupture.

It is important to point out that the number of investigated cases is small at this moment, still preventing general statements regarding the role of shear related to intracranial aneurysm rupture. Additional aneurysm datasets need to be simulated and quantitatively evaluated. However, all five aneurysms considered in this study were patient-specific and simulated in large, connected computational domains. Although this is computationally more expensive, it is a more realistic approach in comparison to studies where only the affected area is investigated.

V. Conclusion and Outlook

The investigation of these two diseased intracranial vascular systems indicates that, although low as well as high shear regions are found, an aneurysmal rupture cannot be explained exclusively by this single hemodynamic parameter. Neither temporal-averaged wall shear stresses, nor their gradients show significant differences in ruptured or unruptured cases. Only the oscillatory shear index was elevated in both ruptured cases, but one unruptured aneurysm showed increased values as well.

Since the number of investigated cases is still small, further studies containing multiple aneurysms need to be carried out in order to consolidate the described results. In this context quantitative evaluations are necessary to find further correlations between hemodynamic parameters and the life-threatening event of a cerebral aneurysm rupture.

Acknowledgment

The authors would like to express their gratitude to Dr. Oliver Speck and Daniel Stucht (Department of Biomedical

Magnetic Resonance, University of Magdeburg, Magdeburg, Germany) whose support was essential for successful MRI measurements.

Furthermore, special thanks are addressed to Dr. Michael Markl (Department of Radiology and Biomedical Engineering, Northwestern University Feinberg School of Medicine, Chicago, USA) and his group for developing and providing the tool used to support data extraction from flow data measured via 4D PC-MRI.

REFERENCES

[1] J. L. Brisman, J. K. Song, and D. W. Newell, "Cerebral Aneurysms," *N Engl J Med*, vol. 355, pp. 928-939, 2006.

[2] P. R. Chen, K. Frerichs, and R. Spetzler, "Natural history and general management of unruptured intracranial aneurysms," *Neurosurg. Focus*, vol. 17, 2004.

[3] J. T. King Jr., "Epidemiology of aneurysmal subarachnoid hemorrhage," *Neuroimag. Clin. North Am.*, vol. 7, pp. 659-668, 1997.

[4] G. J. Rinkel, M. Djibuti, A. Algra, and J. van Gijn, "Prevalence and risk of rupture of intracranial aneurysms: a systematic review," *Stroke*, vol. 29, pp. 251-256, 1998.

[5] J. Xiang, S. K. Natarajan, M. Tremmel, D. Ma, J. Mocco, L. N. Hopkins, A. H. Siddiqui, E. I. Levy, and H. Meng, "Hemodynamic-morphologic discriminants for intracranial aneurysm rupture," *Stroke*, vol. 42, pp. 144-152, 2011.

[6] T. J. Ingall, J. P. Whisnant, D. O. Wiebers, and W. M. O'Fallon, "Has there been a decline in subarachnoid hemorrhage mortality?," *Stroke*, vol. 20, pp. 718-724, 1989.

[7] J. Raymond, D. Roy, A. Weill, F. Guilbert, T. Nguyen, A. J. Molyneux, A. J. Fox, S. C. Johnston, J. P. Collet, and I. Rouleau, "Unruptured intracranial aneurysms and the Trial on Endovascular Aneurysm Management (TEAM): The principles behind the protocol," *Journal of Vascular and Interventional Neurology*, vol. 1, pp. 22-26, 2008.

[8] N. H. Bigelow, "Multiple intracranial arterial aneurysms; an analysis of their significance," *AMA Arch Neurol Psychiatry*, vol. 73, pp. 76-99, 1955.

[9] W. McKissock, A. Richardson, L. Walsh, and E. Owen, "Multiple intracranial aneurysms," *Lancet*, vol. 15, pp. 623-626, 1964.

[10] R. J. Andrews and P. K. Spiegel, "Intracranial aneurysms. Age, sex, blood pressure, and multiplicity in an unselected series of patients," *J Neurosurg*, vol. 51, pp. 27-32, 1979.

[11] K. Mizoi, T. Yoshimoto, Y. Nagamine, T. Kayama, and K. Koshu, "How to treat incidental cerebral aneurysms: a review of 139 consecutive cases," *Surg Neurol*, vol. 44, pp. 114-120, 1995.

[12] T. Inagawa, "Surgical treatment of multiple intracranial aneurysms," *Acta Neurochir*, vol. 108, pp. 22-29, 1991.

[13] J. Rinne *et al.*, "Multiple intracranial aneurysms in a defined population: prospective angiographic and clinical study," *Neurosurgery*, vol. 35, pp. 803-808, 1994.

[14] T. Inagawa, "Multiple intracranial aneurysms in elderly patients," *Acta Neurochir*, vol. 106, pp. 119-126, 1990.

[15] J. R. Østergaard and E. Høg, "Incidence of multiple intracranial aneurysms: influence of arterial hypertension and gender," *J Neurosurg*, vol. 63, pp. 49-55, 1985.

[16] J. Cebral, F. Mut, M. Raschi, E. Scrivano, R. Ceratto, P. Lylyk, and C. Putman, "Aneurysm rupture following treatment with flow-diverting stents: Computational hemodynamics analysis of treatment," *American Journal of Neuroradiology*, vol. 32, pp. 27-33, 2011.

[17] H. Meng *et al.*, "Complex hemodynamics at the apex of an arterial bifurcation induces vascular remodeling resembling cerebral aneurysm initiation," *Stroke*, vol. 38, pp. 1924-1931, 2007.

[18] J. Cebral, F. Mut, J. Weir, and C. Putman, "Quantitative characterization of the hemodynamic environment in ruptured and unruptured brain aneurysms," *American Journal of Neuroradiology*, vol. 32, pp. 145-151, 2011.

[19] D. Fiorella, C. Sadasivan, H. H. Woo, and B. Lieber, Regarding "Aneurysm Rupture Following Treatment with Flow-Diverting Stents: Computational Hemodynamics Analysis of Treatment," *Am J Neuroradiol*, vol. 32, pp. E95-E97, 2011.

[20] J. Alastruey, K. H. Parker, J. Peiró, S. M. Byrd, and S. J. Sherwin, "Modelling the circle of Willis to assess the effects of anatomical variations and occlusions on cerebral flows," *Journal of Biomech*, vol. 40, pp. 1794-805, 2007.

[21] M. A. Castro, C. M. Putman, and J. R. Cebral, "Computational fluid dynamics modeling of intracranial aneurysms: effects of parent artery segmentation on intra-aneurysmal hemodynamics," *Am J Neuroradiol*, vol. 27, pp. 1703-1709, 2006.

[22] A. Marzo, P. Singh, I. Larrabide, A. Radaelli, S. Coley, M. Gwilliam, I. D. Wilkinson, P. Lawford, P. Reymond, U. Patel, A. Frangi, and D. R. Hose, "Computational hemodynamics in cerebral aneurysms: The effects of modeled versus measured boundary conditions," *Annals of Biomedical Engineering*, vol. 39, pp. 884-896, 2011.

[23] D. Zuleger, D. Poulikakos, A. Valavanis, and S. Kollias, "Combining magnetic resonance measurements with numerical simulations – Extracting blood flow physiology information relevant to the investigation of intracranial aneurysms in the circle of Willis," *International Journal of Heat and Fluid Flow*, vol. 31, pp. 1032-1039, 2010.

[24] T. Mönch, M. Neugebauer, and B. Preim, "Optimization of Vascular Surface Models for Computational Fluid Dynamics and Rapid Prototyping" in *Proc. Second International Workshop on Digital Engineering*, Magdeburg, Germany, 2011, pp. 16-23.

[25] M. Neugebauer, G. Janiga, O. Beuing, M. Skalej, and B. Preim, "Computer-aided modelling of blood flow for the treatment of cerebral aneurysms," *International Journal of Biomedical Engineering and Technology*, vol. 55, pp. 37-41, 2010.

[26] P. Berg, G. Janiga, and D. Thévenin, "Detailed Comparison Of Numerical Flow Predictions In Cerebral Aneurysms Using Different CFD Software," in *Proc. Conference on Modelling Fluid Flow (CMFF)*, Budapest, Hungary, 2012, pp. 128-135.

[27] P. Berg, G. Janiga, and D. Thévenin, "Investigation Of The Unsteady Blood Flow In Cerebral Aneurysms With Stent Using The Open-source Software OpenFOAM®," in *Proc. Open Source CFD International Conference (OSCIC)*, Chantilly, France, 2011, pp. 1-8.

[28] A. F. Stalder, M. F. Russe, A. Frydrychowicz, J. Bock, J. Hennig, and M. Markl, "Quantitative 2D and 3D phase contrast MRI: Optimized analysis of blood flow and vessel wall parameters," *Magn Reson Med*, vol. 60, pp. 1218–1231, 2008.

[29] A. Valencia, D. Ledermann, R. Rivera, E. Bravo, and M. Galvez, "Blood flow dynamics and fluid–structure interaction in patient-specific bifurcating cerebral aneurysms," *Int J Numer Meth Fluids*, vol. 58, pp. 1081-1100, 2008.

[30] V. L. Rayz and S. A. Berger, "Computational Modeling of Vascular Hemodynamics," in *Computational Modeling in Biomechanics*, S. De, F. Guilak, M. Mofrad, Ed., Berlin Heidelberg: Springer, New York, 2010, pp. 171-206.

[31] Y. Huo, T. Wischgoll, and G. S. Kassab, "Flow patterns in three-dimensional porcine epicardial coronary arterial tree," *Am. J. Physiol Heart Circ Physiol*, vol. 293, pp. H2959–H2970, 2007.

Philipp Berg lives in Magdeburg, Germany, which is the capital of Saxony-Anhalt and approximately 150 km in the west of Berlin. He was born in the same city on November 6, 1985. Between 2005 and 2011, he studied mechanical engineering with a major in numerics at the University of Magdeburg, the University of Ottawa (Canada) and the University of Niigata (Japan). In the beginning of 2011, he finished his studies with distinction as Dipl.-Ing. of mechanics.

He has worked for the Volkswagen AG (Braunschweig, Germany) in 2010, investigating the pressure drop in dampers. At present, he is working as research assistant at the Department of Fluid Dynamics and Technical Flows, University of Magdeburg. His PhD topic is related to the numerical investigation of the hemodynamics in intracranial aneurysms. In the focus of interest are rupture prediction as well as stenting optimization.

Mr. Berg is member of the American Society of Mechanical Engineering (ASME) and received best paper awards for the following publications:
P. Berg, O. Beuing, G. Janiga, M. Neugebauer, M. Skalej and D. Thévenin, "Characterization Of The Ruptured Site In Intracranial Aneurysms Based On CFD Computations", In *Proc. Computer Methods in Biomechanics and Biomedical Engineering (CMBBE)*, Berlin, Germany, 339-344, 2012
P. Berg, G. Janiga and D. Thévenin, „Instationäre Strömungssimulationen und Auswertung von Blutströmungen in zerebralen Aneurysmen mit Stent", In *Proc. Computer- und Roboterassistierte Chirurgie (CURAC)*, Magdeburg, Germany, ISBN 978-3-940961-59-4, 91-94, 2011.